Tunable Orbital Angular Momentum Radiation
from Angular-Momentum-Biased Microcavities

Adam Mock

School of Engineering and Technology and Science of Advanced Materials Program,
Central Michigan University, Mount Pleasant, Michigan 48859, USA

Dimitrios Sounas

Department of Electrical and Computer Engineering, The University of Texas at Austin, Austin, Texas 78712, USA

Andrea Alù

Department of Electrical and Computer Engineering, The University of Texas at Austin, Austin, Texas 78712, USA
and Advanced Science Research Center, City University of New York, New York, New York 10031, USA

Lasers and light emitters do not typically radiate fields with orbital angular momentum (OAM). Here we show that a suitable scheme of spatiotemporal modulation of a microring cavity laser can impart a synthetic angular momentum, resulting in beams with well-defined OAM. The phenomenon relies on a traveling wave modulation of the refractive index of the microring, which breaks the degeneracy of oppositely oriented whispering gallery modes. In parallel, a static structural grating on the periphery of the microring enables efficient vertical radiation. The proposed structure is inherently tunable and can also emit fields with zero net OAM while retaining toroidal energy distributions similar to the effect of an axicon lens.

Modern optical communication systems exploit various electromagnetic wave properties to increase the bit rate per unit carrier frequency. Traditional approaches exploit polarization and phase diversity. Recently, orbital optical angular momentum (OAM) has shown promise as an additional degree of freedom to increase spectral efficiency [1,2]. Because there is no physical limit on the OAM order that one can radiate, in theory OAM provides an unlimited number of additional communication channels for any given system. In practice, the number of OAM channels is limited by diffraction and by the ability to create and detect waves with well-defined OAM order. Traditional light sources do not possess net angular momentum, so, by conservation of angular momentum, the emitted radiation will also not contain net OAM, though there could be emitted equal amounts of positive and negative angular momentum such as in a higher order vertical cavity surface emitting laser (VCSEL) mode. In this paper, we put forth a technique for electrically biasing a ring resonator cavity with a net angular momentum, which subsequently emits radiation with well-defined and tunable OAM signature.

In previous studies, OAM laser beams have been created from beams without OAM by passing through spiral phase plates or forked linear gratings [3]. Other approaches have exploited metasurfaces [4,5], spatial light modulators [6], and *q* plates [7,8]. Cai *et al.* demonstrated OAM beams generated from notched microring resonators sourced by light coupled from a bus waveguide [9]. A single whispering gallery mode (either clockwise or counterclockwise) was excited by a unidirectional wave from the bus waveguide, and the resonators emitted the OAM radiation vertically. Other integrated optics approaches for generating OAM radiation include an Archimedean spiral-shaped waveguide [10–12], a collection of subwavelength cavities designed for broadband OAM vertical radiation [13] and phased array nanoantennas [14]. In these designs, however, the light source and the OAM generating element are two discrete components. A single, compact laser device with nondegenerate modes possessing nontrivial OAM would reduce cost, improve efficiency, and enable a larger degree of integration.

In this context, a recent study demonstrated a microring OAM laser by exploiting $\mathcal{PT}$ symmetry [15]. Introducing appropriately spaced gain and loss regions along the microring results in a complex grating whose Fourier decomposition has a single complex component rather than the usual two, enabling symmetry breaking and the selective excitation of one OAM order [16]. However, this approach inherently requires absorbing elements in the resonator, which expectedly increases the laser threshold. Furthermore, the need of heterogeneous materials deposited on the ring in order to establish separate gain and loss regions complicates scalability and integration with other components.

In the following, we present a cavity design capable of vertically emitting tunable OAM beams using a spatiotemporally modulated microring cavity. Our design is
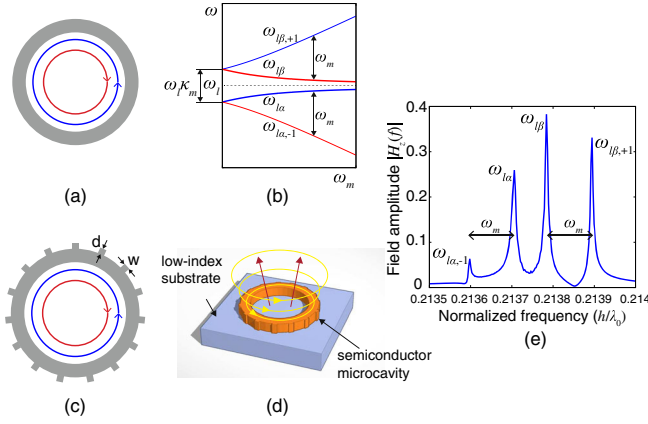
FIG. 1. (a) Schematic diagram depicting a microring resonator and the directionality of two degenerate whispering gallery modes. (b) Dependence of the characteristic frequencies on modulation frequency ω_m of the four components resulting from spatiotemporal modulation. (c) Top view of the OAM laser cavity showing a static structural grating on the periphery of the microring. (d) Three-dimensional depiction of the vertical emission of OAM radiation. (e) Detailed view of resonance spectrum in the vicinity of $h/\lambda_0 = 0.2137$ where h is the cavity height. Spectrum was obtained by taking the discrete Fourier transform of a time sequence calculated by the three-dimensional finite-difference time-domain method and fitted using Padé approximants [24].

based on an InGaAsP material system, making it amenable to optical communication systems operating at $\lambda_0 = 1.55 \ \mu m$. The approach does not require additional absorptive regions added to the microring, and the modulated microring cavities maintain large quality (Q) factors in excess of 20 000. This makes the cavity a good candidate for electrically pumped continuous-wave OAM laser operation. One may also envision the extension of these concepts to all-optical modulation exploiting nonlinearities.

Consider the microring resonator schematically depicted in Fig. 1(a). Such a resonator supports pairs of degenerate states with positive and negative angular momentum $|+l\rangle$ and $|-l\rangle$ with frequency $\omega_{+l} = \omega_{-l} \equiv \omega_l$. One could imagine mechanically spinning this cavity about its central vertical axis, and the ensuing Doppler effect would break the degeneracy between $|+l\rangle$ and $|-l\rangle$. The resultant frequency-separated modes would then radiate fields with distinct OAM orders. In most scenarios, mechanically spinning the cavity is impractical and would require very large angular velocities to experience significant splitting. Alternatively, a synthetic angular momentum can be imparted to the cavity by modulating the electrical permittivity with a traveling wave grating of the form $\Delta\varepsilon(\varphi,t) = \Delta\varepsilon_m \cos(\omega_m t - L_m\varphi)$ [17,18]. The modes $|+l\rangle$ and $|-l\rangle$ can be targeted specifically by choosing $L_m = 2l$. Based on an electromagnetic time-dependent perturbation theory [19,20], the states of the system under modulation assume the form $|l\alpha\rangle = a_{+l}(t)|+l\rangle + a_{-l}(t)|-l\rangle$, where $|l\alpha\rangle$ is a hybridized state consisting of a superposition of

$|+l\rangle$ and $|-l\rangle$. With this modulation, the coefficients $a_{+l}(t)$ and $a_{-l}(t)$ obey the coupled mode equations

$$\dot{a}_{+l}(t) = \left(-i\omega_l - \frac{1}{\tau}\right)a_{+l}(t) - i\frac{\omega_l\kappa_m}{2}e^{-i\omega_m t}a_{-l}(t), \quad (1)$$

$$\dot{a}_{-l}(t) = \left(-i\omega_l - \frac{1}{\tau}\right)a_{-l}(t) - i\frac{\omega_l\kappa_m}{2}e^{i\omega_m t}a_{+l}(t), \quad (2)$$

where τ is the photon lifetime, and $\kappa \sim \int_{-\infty}^{\infty}\int_0^{\infty}\Delta\varepsilon_m \times |E_{tl}(r,z)|^2 rdrdz$ is a unitless coupling coefficient proportional to the overlap integral of the field with the grating, where $E_{tl}(r,z)$ is the field in the cross section (r-z plane) of the unperturbed microring [17,18,20]. Solving Eqs. (1) and (2) results in modes that consist of superpositions of $|+l\rangle$ and $|-l\rangle$ with frequencies separated by ω_m and also different amplitudes. Complete expressions for the two modes resulting from angular momentum bias are

$$|l\alpha\rangle = |+l\rangle e^{-i\omega_{l\alpha}t} + \frac{\Delta\omega}{\omega_l\kappa_m}|-l\rangle e^{-i(\omega_{l\alpha}-\omega_m)t}, \quad (3)$$

$$|l\beta\rangle = -\frac{\Delta\omega}{\omega_l\kappa_m}|+l\rangle e^{-i(\omega_{l\beta}+\omega_m)t} + |-l\rangle e^{-i\omega_{l\beta}t}, \quad (4)$$

where $\omega_{l\alpha} = \omega_l - i(1/\tau) + (\Delta\omega/2)$, $\omega_{l\beta} = \omega_l - i(1/\tau) - (\Delta\omega/2)$ and $\Delta\omega = \omega_m - \sqrt{\omega_m^2 + (\omega_l\kappa_m)^2}$ [17,18,20]. The use of the Dirac ket notation here deviates somewhat from its standard use in quantum mechanics due to the dissipative nature of the resonator modes. Namely, the states cannot be normalized since as $t \to \infty$ all coefficient amplitudes decay to zero. To rectify this formally, a term representing coupling to radiation modes should be included in Eqs. (1) and (2). However, to maintain our present focus on the resonator modes and to be consistent with previous theoretical treatments of electromagnetic coupled mode theory [19], this external coupling will be neglected.

Figure 1(b) shows the evolution of the frequencies of the modulated ring modes versus ω_m keeping in mind that each mode contains two frequency components: $\omega_{l\alpha}$ and $\omega_{l\alpha,-1} \equiv \omega_{l\alpha} - \omega_m$ are the frequency components of the mode $|l\alpha\rangle$, while $\omega_{l\beta}$ and $\omega_{l\beta,+1} \equiv \omega_{l\beta} + \omega_m$ are the frequencies for the mode $|l\beta\rangle$. The terms occurring at frequencies $\omega_{l\alpha}$, $\omega_{l\beta}$ are the components with the largest amplitude. In an example experimental scenario, if the system were to lase at $\omega_{l\alpha}$, then there will also be radiation with opposite angular momentum at $\omega_{l\alpha,-1}$. This fact can possibly be used for communications over separate frequency channels. The two fundamental frequencies $\omega_{l\alpha}$, $\omega_{l\beta}$ approach ω_l as ω_m increases, while $\omega_{l\alpha,-1}$ and $\omega_{l\beta,+1}$ are further displaced from ω_l. It is interesting that, within the context of the coupled mode analysis, these four modes retain the same photon lifetime as the original degenerate WGM modes. This suggests that the spatiotemporal

modulation scheme imparting the desired form of angular momentum does not adversely affect the Q factor of these cavities, which is important for laser applications. In previous work, this degeneracy breaking induced by an angular momentum bias was exploited to realize a magnet-free nonreciprocal component [18]. Here, we show that the imparted effective angular momentum may be used to realize efficient OAM generation, not having to rely on loss and absorption, and directly amenable to integrated laser sources.

The cavity designed for lasing in well-defined OAM modes is shown in Figs. 1(c)–1(d), whose dominant radiation is in the vertical direction. In order to realize vertical radiation, a static structural grating is introduced along the periphery of the microring [9,15]. From standard coupled mode analysis, it can be shown [9,20] that the OAM of the cavity mode l_{wgm} and the OAM of the radiated field l_{rad} are related by

$$l_{rad} = l_{wgm} - gq, \qquad (5)$$

where g is an integer and q is the number of static structural grating periods.

We model the electrodynamics of an angular-momentum-biased microring cavity using three-dimensional (3D) finite-difference time-domain (FDTD) simulations. The ring cavity has a rectangular cross section with height h, thickness $1.5h$, and inner radius $5.5h$. For operation at $\lambda_0 = 1.55\ \mu m$, these geometry specifications become $h = 331$ nm, $1.5h = 497$ nm, and $5.5h = 1.8\ \mu m$. The height and width are consistent with standard semiconductor waveguide geometries. The ring resonator radius is chosen small to keep the simulation domain of reasonable size. These concepts are readily extendable to resonators with larger radii. The cavity has a refractive index $n = 3.17$, consistent with semiconductor active materials [25], and it is bonded to a low index substrate with index $n = 1.74$, consistent with sapphire [26–28]. We introduce a static structural grating with $q = 15$ and $w = d = 0.1h = 33$ nm where w and d are defined in Fig. 1(c). Figure 1(e) shows the passive (no internal absorption or gain) cavity spectrum calculated via discrete Fourier transform of the FDTD time sequence initialized by a spatiotemporal impulse. The set of modes shown in the spectrum possess angular momenta $l_{wgm} = \pm 20$. Four resonance peaks are found, and these peaks correspond to the four frequencies discussed previously and whose dependence on ω_m is depicted in Fig. 1(b). The spatiotemporal bias has an amplitude $\Delta\varepsilon = 0.032$, or $\Delta n = 0.005$, consistent with carrier injection in semiconductor gain materials [29] and a factor of 2 smaller than the index contrast used in a previous approach [15]. The modulation frequency is $\omega_m(h/2\pi c) = 1.08 \times 10^{-4}$, where c is the vacuum speed of light. This comes out to 5×10^{-4} times the optical frequency or $f_m = 100$ GHz at $\lambda_0 = 1.55\ \mu m$.
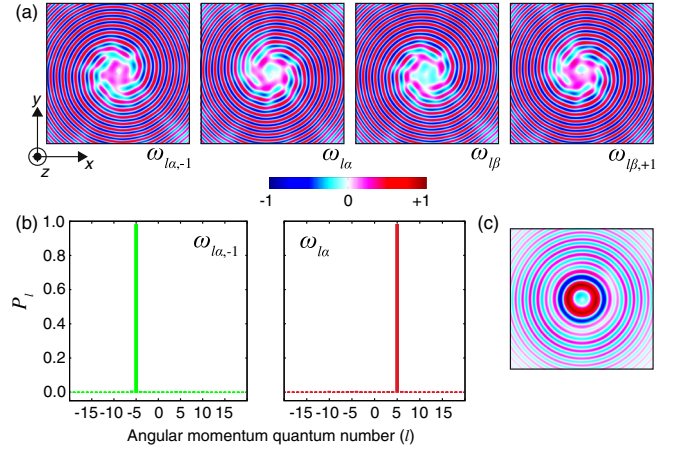

FIG. 2. (a) Field distributions $E_r(x, y, z = 40h)$ calculated using a far-field transformation of the field obtained from FDTD just above the cavity. The width of the view shown is $305h$. (b) Distribution of power in the components of the Fourier-Bessel decomposition Eq. (7). (c) Field distribution $E_r(x, y, z = 40h)$ of a radiation field with OAM $l = 0$ calculated using a far-field transformation of the field obtained from FDTD just above the cavity. The width of the view shown is $305h$.

Interestingly, as we show in the following, despite the huge contrast between modulation and signal frequencies, the modulation enables degeneracy lifting and successfully provides a scheme to realize OAM laser generation.

Figure 2(a) shows $E_r(x, y, z = 40h)$ obtained via a far-field transformation of the FDTD-calculated fields recorded just above the microring (r is the radial component in cylindrical coordinates) for the four resonant peaks in Fig. 1(e) [30]. The resonator mode is TE$_z$-like, in which E_r and H_z are the fundamental field components. In the far-field, the dominant field components are E_r and H_φ (see Ref. [20] for more discussion on the polarization state of the radiated field). The peak amplitudes shown in Fig. 1(e) are determined by Eqs. (3) and (4) but also by the particular method of field excitation and the field monitoring location. To verify Eqs. (3) and (4), the fields shown in Fig. 2(a) can be used. The higher order mode fields ($\omega_{l\alpha,-1}$, $\omega_{l\beta,+1}$) have maximum amplitudes that are 0.51 times the maximum amplitudes of the fundamental mode fields. From the frequency spacing in Fig. 1(e), one obtains $\omega_l\kappa_m = 1.58 \times 10^{-4}$, which yields $(\Delta\omega/\omega_l\kappa_m) = 0.52$ and agrees well with the fields obtained via FDTD.

The left and right handedness of the fields shown in Fig. 2(a) is apparent, and it is consistent with the OAM of the four modes, following the theoretical analysis above [i.e., $|l_{rad}| = |20 - (1)15| = 5$ for the mode with frequency $\omega_{l\alpha}$]. The quality of OAM of the different modes is assessed by calculating the components of a Fourier-Bessel decomposition of the fields. Assuming that

$$E_r(r, \varphi, z_0) = \sum_l d_l J_l(kr) e^{il\varphi}, \qquad (6)$$

the d_l are obtained via

$$d_l = \int_0^{2\pi} \int_0^{\infty} E_r(r, \varphi, z_0) J_l(kr) e^{-il\varphi} r dr d\varphi. \quad (7)$$

Figure 2(b) shows the normalized power in each mode, calculated according to $P_l = |d_l|^2 / \sum_{l'} |d_{l'}|^2$. The coefficients for the $\omega_{l\alpha,-1}$ and $\omega_{l\alpha}$ modes are shown. $P_{-5} = 0.977$ for $\omega_{l\alpha,-1}$ and $P_5 = 0.980$ for $\omega_{l\alpha}$, which indicates that these fields have extremely well-defined OAM. The coefficients for $\omega_{l\beta}$ and $\omega_{l\beta,+1}$ also follow the same trend. The OAM value of $l_{\text{rad}} = \pm 5$ is consistent with the intended value predicted by Eq. (5) in which $l_{wgm} = \pm 20$ and $q = 15$. The grating also scatters the cavity mode into higher order OAM orders, such as $l_{\text{rad}} = 20 - (-1)15 = 35$ and $l_{\text{rad}} = 20 - (2)15 = -10$; however, these modes fall outside the light cone and are not efficiently radiated [9,20].

The Q factor of the $l_{wgm} = 20$ degenerate modes of the ring resonator cavity without modulation and without a static structural grating is $Q = 48\,000$, limited by bend loss and substrate radiation. When a spatiotemporal modulation is applied without a structural grating, the Q factors of the ensuing four modes remain in the range $44\,000$–$50\,000$, which is close to the nominal value and consistent with the theory laid out previously. The purpose of the static grating is to enhance vertical radiation, so the Q factors of the relevant modes will necessarily decrease. In the results presented above, a grating with size parameters $d = w = 0.1h$ maintained the Q factors of the fundamental modes ($\omega_{l\alpha}$ and $\omega_{l\beta}$) to values near $50\,000$. However, the Q factors of the higher order modes $\omega_{l\alpha,-1}$ and $\omega_{l\beta,+1}$ decreased to $27\,000$ and $35\,000$, respectively. The precise reason for these lower Q factor values was not investigated; however, they remain sufficiently high for laser applications. Ultimately, the mode with the highest Q factor and strongest spectral alignment with the gain spectrum will be the lasing mode, and the far field will be dominated by only one set of frequencies ($\omega_{l\alpha}$, $\omega_{l\alpha,-1}$) or ($\omega_{l\beta}$, $\omega_{l\beta,+1}$) depicted in Fig. 1(e), following the laser dynamics.

When the cavity mode of interest has an angular momentum quantum number equal to that of the static structural grating, then $l_{\text{rad}} = l_{wgm} - gq = 0$, and one anticipates a beam with a toroidal field distribution. Figure 2(c) shows the field radiated from a cavity with $q = 15$ and a spatiotemporal modulation with $L_m/2 = 15$. The emitted field maintains a toroidal field distribution, an effect similar to that of an axicon lens [20]. A uniform ring field with zero OAM, such as the one shown in Fig. 2(c), is of potential interest in optical trapping and stimulated emission electron depletion microscopy.

In order to impart a dynamic traveling-wave grating in the microring, the material should be electrically contacted with appropriate resolution. If the continuous azimuthal variation is approximated with discrete stepwise contact points, the Nyquist sampling theorem dictates that at least two samples per period are required. In the present example with $L_m = 2l = 40$, this translates to 80 electrical contact points along the ring, which would be a formidable fabrication demand. However, a previous experimental demonstration of a $\mathcal{PT}$ symmetric OAM laser showed microring cavities with periodic layers of refractive index alternating materials at 56 locations along the ring [15]. While by no means trivial, such fine-scale material control of microring cavities is, in principle, feasible, and complicated junction geometries with multiple interdigitated junctions [31–35] and multiple contact points [36,37] have been experimentally realized in the context of optical modulators. Further, as pointed out in previous work [18], by exploiting the stepwise contact arrangement and Fourier decomposing the individual rect-function contact geometries, one can reduce the total electrical contact number to as little as 3 at the expense of requiring larger modulation amplitude. In the present study, we found that 17 discrete contact points reliably generated good quality OAM beams, even considering the realistic diffusion in the different regions, though simulation time, rather than
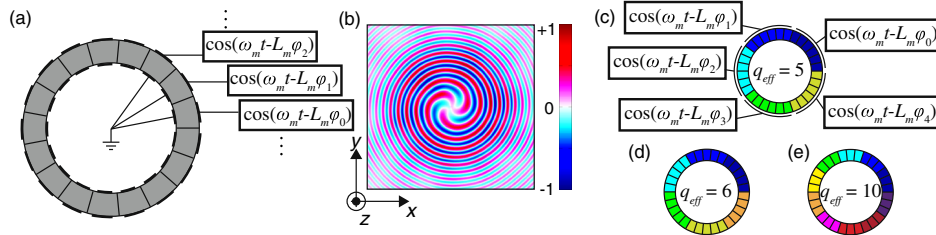

FIG. 3. (a) Schematic depiction of a cavity with 17 discrete modulation contact points. The associated signal applied to the ring is shown for the first three sections. $\varphi_n = (n + 1/2)(2\pi/17)$ for $n = 0\ldots16$. (b) Field distribution $E_r(x, y, z = 40h)$ for the $\omega_{l\alpha,-1}$ mode in the cavity shown in (a) calculated using a far-field transformation of the field obtained from FDTD just above the cavity. The width of the view shown is $305h$. (c) Strategy for dynamically changing the scattering grating period. Rather than applying a different signal to each individual section, adjacent sections can be grouped together, so that the cavity modes are scattered from gratings with larger periods. Five groups of six sections are shown. (d) Same as (c) but with six groups of five sections (modulation signals not shown). (e) Same as (d) but with ten groups of three sections.

fundamental device properties, was the limiting factor. The device geometry is shown schematically in Fig. 3(a), and Fig. 3(b) shows $E_r(x, y, z = 40h)$ for the $\omega_{l\alpha,-1}$ mode of this discrete-modulated cavity with a static structural grating with $q = 17$ and $d = w = 0.2h$. The $l = -3$ OAM signature (resulting from $l_{wgm} = -20$) is apparent with $P_{-3} = 0.982$. More details of this discrete modulation scenario are discussed in Ref. [20].

While reducing the number of electrical contact points on the microring cavity reduces fabrication demands, increasing the number of contact points enables OAM tunability. This is because the periodic discontinuity of refractive index between discrete modulation points creates an effective static grating. In the example shown in Figs. 3(a) and 3(b) we show a field with OAM $l_{\rm rad} = -20 + 17 = -3$, resulting from the 17 discrete contact points. However, if a nonprime number of contact points is used such as $N = 30$, then the emitted OAM can be tuned by applying the same modulation signal to adjacent discrete sections. This is illustrated in Figs. 3(c)–3(e). In Fig. 3(c), groups of six adjoining contacts receive the same modulation signal, thereby reducing the number of effective grating periods from 30 to $q_{\rm eff} = 5$. In this case, the radiated beams would posses OAM with $l_{\rm rad} = -20 + g5$, and only the OAM orders falling within the radiation cone would be coupled out [9,20]. For this specific example, they correspond to $3 \leq g \leq 5$; however, the lowest value of g will dominate, so this configuration would radiate OAM beams predominantly with $l_{\rm rad} = -5$. A similar analysis applies to the devices shown in Figs. 3(d) and 3(e) where $q_{\rm eff} = 6$ and $q_{\rm eff} = 10$, respectively. In those cases, OAM beams with $l_{\rm rad} = -8$ and $l_{\rm rad} = 0$ would be emitted, respectively. The full range of OAM tunability of this device includes OAM orders $l_{\rm rad} = -5, -8, 0, 10$. Similar to the static structural gratings discussed above, the Q factors of these cavities remain close to their unperturbed values.

To conclude, a new approach to impart OAM to microcavity laser emission has been presented, which does not require the use of loss to balance gain, as in previous demonstrations. The proposed design is based on azimuthal spatiotemporal modulation of a microring cavity, which lifts the degeneracy of clockwise and counterclockwise whispering gallery modes. The radiated OAM can be dynamically tuned by controlling the electrical signal applied to the discrete modulation sections. The design maintains the high Q factors of these cavities and only moderate modulation amplitudes and frequencies are needed. This approach also avoids the introduction of lossy materials into the cavity, as it is required for OAM lasers based on $\mathcal{PT}$ symmetry. Applications of this OAM microlaser include OAM multiplexing in optical communications, optical trapping, and manipulation and stimulated emission depletion microscopy. We also point out that the proposed laser cavities are inherently nonreciprocal, similar to recently proposed spatiotemporally modulated

antennas [38], which leads to the added potential benefit of eliminating the need for an additional protective optical isolator device.

[1] F. Tamburini, E. Mari, A. Sponselli, B. Thidé, A. Bianchini, and F. Romanato, New J. Phys. **14**, 033001 (2012).

[2] J. Wang, J.-Y. Yang, I. M. Fazal, N. Ahmed, Y. Yan, H. Huang, Y. Ren, Y. Yue, S. Dolinar, M. Tur, and A. E. Willner, Nat. Photonics **6**, 488 (2012).

[3] A. M. Yao and M. J. Padgett, Adv. Optics Photonics **3**, 161 (2011).

[4] N. Yu, P. Genevet, M. A. Kats, F. Aieta, J.-P. Tetienne, F. Capasso, and Z. Gaburro, Science **334**, 333 (2011).

[5] G. Li, M. Kang, S. Chen, S. Zhang, E. Y. -B. Pun, K. W. Cheah, and J. Li, Nano Lett. **13**, 4148 (2013).

[6] G. Gibson, J. Coutial, M. J. Padgett, M. Vasnetsov, V. Pas'ko, S. M. Barnett, and S. Franke-Arnold, Opt. Express **12**, 5448 (2004).

[7] L. Marrucci, C. Manzo, and D. Paparo, Phys. Rev. Lett. **96**, 163905 (2006).

[8] D. Naidoo, F. S. Roux, A. Dudley, I. Litvin, B. Piccirillo, L. Marrucci, and A. Forbes, Nat. Photonics **10**, 327 (2016).

[9] X. Cai, J. Wang, M. J. Strain, B. Johnson-Morris, J. Zhu, M. Sorel, J. L. O'Brien, M. Thompson, and S. Yu, Science **338**, 363 (2012).

[10] G. Rui, R. L. Nelson, and Q. Zhan, Opt. Express **20**, 18819 (2012).

[11] S. Mochizuki, X. Gu, K. Tanabe, A. Matsutani, M. Ahmed, A. Bakry, and F. Koyama, Appl. Phys. Express **7**, 022502 (2014).

[12] S. Li, W. Yu, L. Meriggi, Q. Xiao, Z. Nong, Z. Cai, M. Sorel, and S. Yu, Opt. Lett. **42**, 975 (2017).

[13] Z. Xie, T. Lei, F. Li, H. Qiu, Z. Zhang, H. Wang, C. Min, L. Du, Z. Li, and X. Yuan, arxiv:1703.04311.

[14] J. Sun, M. Moresco, G. Leake, D. Coolbaugh, and M. R. Watts, Opt. Lett. **39**, 5977 (2014).

[15] P. Miao, Z. Zhang, J. Sun, W. Walasik, S. Longhi, N. M. Litchinitser, and L. Feng, Science **353**, 464 (2016).

[16] L. Feng, Y.-L. Xu, W. S. Fegadolli, M.-H. Lu, J. E. B. Oliveira, V. R. Almeida, Y.-F. Chen, and A. Scherer, Nat. Mater. **12**, 108 (2013).

[17] D. L. Sounas, C. Caloz, and A. Alù, Nat. Commun. **4**, 2407 (2013).

[18] D. L. Sounas and A. Alù, ACS Photonics **1**, 198 (2014).

[19] J. N. Winn, S. Fan, J. D. Joannopoulos, and E. P. Ippen, Phys. Rev. B **59**, 1551 (1999).

[20] See Supplemental Material at http://link.aps.org/supplemental/10.1103/PhysRevLett.121.103901 for derivation of Eqs. (1)–(4), derivation of Eq. (5), discussion of spin and orbital angular momentum, discussion of Fourier-Bessel decomposition of beams with OAM $l = 0$, details on discrete modulation scheme, coupling to radiation modes, and which includes Refs. [21–23].

[21] A. Niv, G. Biener, V. Kleiner, and E. Hasman, Opt. Express **14,** 4208 (2006).

[22] L. Huang, X. Chen, H. Mühlenbernd, G. Li, B. Bai, Q. Tan, G. Jin, T. Zentgraf, and S. Zhang, Nano Lett. **12,** 5750 (2012).

[23] M. Khorasaninejad and K. B. Crozier, in *Conference on Lasers and Electro-Optics Technical Digest, San Jose, CA, 2014*, p. SF10.2.

[24] A. Mock and J. D. O'Brien, Opt. Quantum Electron. **40,** 1187 (2008).

[25] N. Suzuki and K. Tada, Jpn. J. Appl. Phys. **23,** 291 (1984).

[26] J. R. Cao, W. Kuang, Z.-J. Wei, S.-J. Choi, H. Yu, M. Bagheri, J. D. O'Brien, and P. D. Dapkus, IEEE Photonics Technol. Lett. **17,** 4 (2005).

[27] M. H. Shih, W. Kuang, T. Yang, M. Bagheri, Z.-J. Wei, S.-J. Choi, L. Lu, J. D. O'Brien, and P. D. Dapkus, IEEE Photonics Technol. Lett. **18,** 535 (2006).

[28] L. Lu, A. Mock, M. Bagheri, J.-R. Cao, S.-J. Choi, J. D. O'Brien, and P. D. Dapkus, IEEE Photonics Technol. Lett. **21,** 1166 (2009).

[29] B. R. Bennet, R. A. Soref, and J. A. Del Alamo, IEEE J. Quantum Electron. **26,** 113 (1990).

[30] A. Taflove and S. C. Hagness, *Computational Electrodynamics*, 3rd ed. (Artech House, Massachusetts, 2005).

[31] X. Xiao, H. Xu, X. Li, Y. Hu, K. Xiong, Z. Li, T. Chu, Y. Yu, and J. Yu, Opt. Express **20,** 2507 (2012).

[32] X. Xiao, X. Li, H. Xu, Y. Hu, K. Xiong, Z. Li, T. Chu, J. Yu, and Y. Yu, IEEE Photonics Technol. Lett. **24,** 1712 (2012).

[33] J. C. Rosenberg, W. M. J. Green, S. Assefa, D. M. Gill, T. Barwicz, M. Yang, S. M. Shank, and Y. A. Vlasov, Opt. Express **20,** 26411 (2012).

[34] M. Pantouvaki, H. Yu, M. Rakowski, P. Christie, P. Verheyen, G. Lepage, N. V. Hoovels, P. Absil, and J. V. Campenhout, IEEE J. Select. Topics Quant. Electron. **19,** 7900308 (2013).

[35] G. T. Reed, G. Z. Mashanovich, F. Y. Gardes, M. Nedeljkovic, Y. Hu, D. J. Thomson, K. Li, P. R. Wilson, S.-W. Chen, and S. S. Hsu, Nanophotonics **3,** 229 (2014).

[36] D. Patel, S. Ghosh, M. Chagnon, A. Samani, V. Veerasubramanian, M. Osman, and D. V. Plant, Opt. Express **23,** 14263 (2015).

[37] A. D. Simard, B. Filion, D. Patel, D. Plant, and S. LaRochelle, Opt. Express **24,** 19467 (2016).

[38] Y. Hadad, J. C. Soric, and A. Alù, Proc. Natl. Acad. Sci. U.S.A. **113,** 3471 (2016).